

A Polarization Hall Effect in Hydrated DNA

Mariusz Pietruszka^{1,*}

¹*University of Silesia, Faculty of Natural Sciences, Institute of Biology, Biotechnology, and Environmental Protection, 40-032 Katowice, Poland*

(Dated: January 13, 2026)

Understanding how biological soft matter responds to electromagnetic fields under ambient conditions remains a central challenge, as thermal fluctuations are generally expected to suppress long-range organization. Here, we report that hydrated DNA exhibits a reproducible magnetic-field-induced transition characterized by a sharp transverse-voltage threshold (~ 40 – 50 mV), followed by a regime of regular, phase-stable oscillations in the transverse polarization signal. These features emerge only beyond the threshold and display a pronounced temperature dependence, consistent with the formation of a collective mode within the hydrogen-bond network of the DNA–water interface. Motivated by recent studies of Hall-like responses carried by neutral excitations, including phonons, magnons, and excitons, we interpret the observed transverse signal in terms of coherent polarization dynamics of proton–proton-hole dipoles confined to a quasi-two-dimensional hydrated layer. Within this framework, the transverse response is attributed to a field-organized polarization mode; the measured transverse voltage arises from collective dipolar dynamics rather than steady carrier transport. These results identify hydrated DNA as a soft-matter system in which magnetic field and temperature jointly modulate collective polarization dynamics, providing a biologically relevant platform for exploring coherence and transverse responses in hydrogen-bonded media.

I. INTRODUCTION

Hydrated DNA forms a structured yet dynamically fluctuating hydrogen-bond network whose collective electrodynamic properties remain only partially understood. At the molecular scale, proton transfer along hydrogen bonds, hydration-layer ordering, and long-range dipolar interactions have been studied extensively, with theoretical models predicting cooperative proton dynamics and correlated vibrational modes in soft biological assemblies [1–5]. These microscopic ideas are complemented by macroscopic frameworks developed to describe coherent or synergistic organization in biological systems [6, 7], as well as by broader discussions of biological coherence and quantum-like behavior [8].

A central open question is whether such collective behavior can persist at mesoscopic scales under ambient conditions, given the well-known constraints imposed by thermal fluctuations and decoherence in biological environments [9]. Most experimental and theoretical studies of DNA electrostatics have focused on ionic conduction in solution or charge migration along π -stacked base pairs, leaving unresolved whether coherent polarization modes might instead arise within the DNA–water interface under external-field excitation. Prior analyses of cooperative protonic and dipolar dynamics in biological matter, together with atomistic simulations of confined hydration layers [5], suggest that a structured hydration shell could, in principle, support correlated dipolar fluctuations. Direct macroscopic evidence for such field-induced collective behavior, however, has remained limited.

Over the past several years, magnetic-field experiments on hydrated DNA have revealed a reproducible pattern

of sudden voltage thresholds, staircase-like plateaus, and oscillatory features at or near room temperature [10–12]. The observed $1/B$ -periodic oscillations bear a formal resemblance to Shubnikov–de Haas behavior known from electronic quantum transport [13–15]. At the same time, the biological context and the absence of sustained charge flow point to a fundamentally different physical mechanism. Control measurements on pure water, desiccated DNA, and ionic or metallic substrates do not reproduce these effects, indicating that the structured DNA hydration layer—rather than conventional electrical conduction—governs the response.

The physical interpretation of these features has therefore required reassessment. Earlier work described the transverse signals in terms of a “protonic Hall effect,” implicitly invoking mobile proton carriers. Subsequent experiments combining magnetic-field sweeps with high-resolution temperature control demonstrated that the transverse response persists even in regimes where no continuous conduction pathway exists. These observations motivated a reinterpretation in which the measured voltages arise from collective polarization dynamics of proton–proton-hole dipoles embedded within the hydrogen-bond network of the hydrated DNA interface.

Importantly, neutral dipolar excitations can exhibit Hall-type transverse responses. In modern condensed-matter physics, it is now well established that neutral quasiparticles—including phonons, magnons, and excitons—can generate Hall-like effects through mechanisms involving Berry curvature, chiral geometry, or broken inversion symmetry [16–23]. These developments provide a natural conceptual bridge: hydrated DNA hosts strongly polarizable protonic dipoles within an intrinsically chiral molecular environment, making a magnetically induced transverse polarization response plausible even in the absence of itinerant charge carriers.

* mariusz.pietruszka@us.edu.pl

From this perspective, hydrated DNA can be viewed as a soft, quasi-two-dimensional dipolar medium whose polarization modes are organized jointly by magnetic field and temperature. The possibility of macroscopic coherence in such dipolar ensembles is consistent with early predictions for driven biological systems [1, 6] and with general principles of phase coherence and mode condensation studied in physical systems, including Bose–Einstein condensates [24, 25]. Although the DNA–water interface operates in a regime very different from ultracold atomic gases, the underlying concept—the emergence of collective phase coherence from coupled degrees of freedom—remains relevant.

In the present work, the hydrated DNA layer acts effectively as a quasi-two-dimensional coherent medium. Its characteristic thickness of approximately $10\ \mu\text{m}$, combined with strong in-plane coupling mediated by the hydration network, confines protonic polarization modes to a planar geometry. This situation is analogous to two-dimensional excitonic, magnonic, and phononic systems, in which magnetic field and reduced dimensionality jointly govern coherence. Such a two-dimensional organization provides the natural context for the quantized oscillations and plateau structures reported here, indicating that the DNA–water interface behaves as a field-organized dipolar ensemble capable of supporting long-range phase coherence.

Here we employ a combined magnetic-field and temperature-control strategy to systematically map coherent regimes in hydrated DNA. By treating magnetic field and temperature as independent control parameters and by monitoring simultaneous longitudinal and transverse responses, we resolve transitions between incoherent fluctuations, SdH-like oscillatory behavior, plateau-like polarization states, and a low-temperature Fröhlich-type coherent mode. Together, these results demonstrate that hydrated DNA supports field-stabilized and temperature-gated polarization coherence, extending the physics of neutral-excitation Hall responses and coherent dipolar ordering to a biologically relevant, hydrogen-bonded soft-matter system.

II. RESULTS

Field-Stabilized and Temperature-Gated Dipolar Coherence in Hydrated DNA

Throughout this work, V_{xy} is treated as a transverse polarization voltage, arising from time-dependent collective dipolar reorientation (dP/dt), and not as a Hall voltage generated by itinerant charge transport.

Oscillatory and quantization-like features are typically discussed in the context of charge transport. Here, we show that an analogous structure can emerge in a soft, hydrated dipolar network, where the relevant degrees of freedom are collective protonic dipoles rather than itinerant charges. In hydrated DNA, hydrogen-bond networks

in the interfacial water and at base-pair sites support proton–proton-hole dipolar pairs that align and oscillate under a magnetic field. The resulting macroscopic observable is a transverse polarization voltage (V_{xy}), proportional to the polarization current ($J = dP/dt$).

Under moderate magnetic fields and ambient conditions, we observe three canonical features in this polarization channel: (i) $1/B$ -periodic polarization oscillations in both V_{xy} and V_{xx} , which act as SdH-like precursors of dipolar quantization (used here as a transport-style formalism rather than evidence of electronic Landau quantization); (ii) a sharp, field-driven threshold marking reorganization of dipolar domains; and (iii) discrete, Landau-like polarization plateaus in V_{xy} .

Both the oscillatory periodicity and the plateau spacing yield convergent estimates of an effective coherence density, $n_{\text{eff}} \approx 4.7 \times 10^{14}\ \text{m}^{-2}$, indicating that a single field-organized dipolar ensemble likely governs the response. A transition near $\sim 0.35\ \text{T}$ marks a reorganization from repeated Landau-like dipolar quantization to a Fröhlich-like phase characterized by long-range, phase-locked dipolar oscillations and simplified response lobes. Control measurements in pure water lack these features, confirming that structured DNA hydration layers are essential.

Throughout this work we retain the quantitative transport-style formalism (e.g., $1/B$ periodicity, filling-factor-style plateaus, and tensor inversion), but interpret the observables within a polarization-response framework. In this view, extracted scales (e.g., densities inferred from periodicities or plateau spacings) parameterize the collective dynamics of a field-organized dipolar ensemble rather than itinerant charge transport. The hydrated DNA interface thus operates as a quasi-two-dimensional dipolar medium in which the magnetic field discretizes polarization modes and stabilizes macroscopic dipolar coherence at room temperature.

Across datasets, the key features (threshold, plateau spacing, and $1/B$ periodicity) recur with consistent scales under varied protocols, supporting a reproducible sample-defined response rather than run-specific readout effects.

Field-induced polarization response in DNA–water matrices

To probe field-induced coherence, we measured the transverse polarization voltage V_{xy} in a quasi-two-dimensional hydrated DNA layer under a perpendicular magnetic field at ambient conditions. Figure 1 provides the microscopic basis adopted throughout: transient proton relays along hydrogen bonds generate locally neutral proton–proton-hole dipoles that align and oscillate cooperatively within the hydration layer. These dipoles experience a Lorentz-like magnetic torque, and their collective reorientation generates a measurable polarization current $J_{\text{pol}} = dP/dt$, detected macroscopically as the transverse voltage V_{xy} . Under moderate magnetic fields

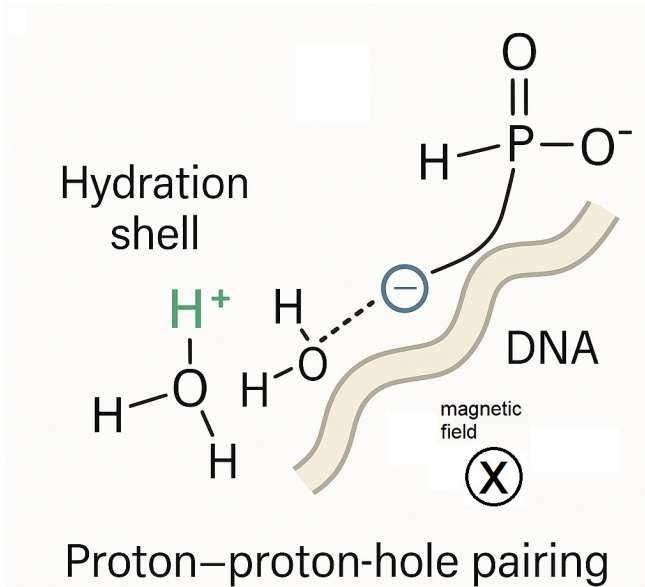


FIG. 1. Conceptual illustration of proton–proton-hole pairing along a DNA–water hydrogen bond. A schematic of a locally neutral proton–proton-hole pair at the DNA–water interface under magnetic field. Transient proton relay (H^+) along a hydrogen bond leaves a correlated proton hole at the donor site; many such dipoles, stabilized by the hydrogen-bond network, align and oscillate collectively. Their synchronized dynamics generate a macroscopic polarization $P(t)$ whose time derivative $J_{\text{pol}} = dP/dt$ is detected as the transverse polarization voltage V_{xy} . The schematic motivates the field-induced coherent polarization mechanism underlying the experiments.

(0.1–0.65 T) and room temperature, this polarization channel exhibits a reproducible progression of features: (i) $1/B$ -periodic oscillations in both V_{xy} and V_{xx} , serving as Shubnikov–de Haas-like precursors of dipolar quantization; (ii) a sharp, field-driven threshold; and (iii) the emergence of discrete, Landau-like polarization plateaus in V_{xy} . The oscillation periodicity and the spacing of these plateaus both yield a convergent coherence density of approximately $4.7 \times 10^{14} \text{ m}^{-2}$, indicating that a single, field-organized dipolar ensemble governs the response. Control measurements in pure water remain featureless under otherwise identical conditions, demonstrating that structured DNA hydration layers are essential for the observed field-induced coherence.

Temperature-driven onset and reorganization of dipolar coherence

To resolve how temperature influences the organization of the dipolar network, we performed continuous cooling sweeps at a fixed magnetic field and monitored both longitudinal (I_{xx} and V_{xx}) and transverse (V_{xy}) polarization channels at 1 Hz sampling. Figures 2 and 3 summarize

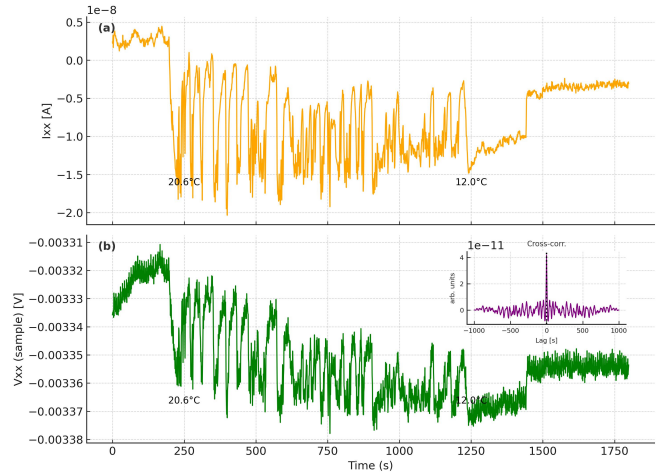


FIG. 2. Temperature-driven reorganization of the longitudinal response in hydrated DNA. A continuous temperature sweep from above 20.6°C down to below 12.0°C reveals two clear transition points in the longitudinal channels of a hydrated DNA–water matrix ($500 \text{ ng}/\mu\text{L}$, $5 \mu\text{L}$, $\text{pH} \approx 8$, $B = 500 \text{ mT}$). (a) The longitudinal current $I_{xx} = V_{xx}/(1 \text{ k}\Omega)$ (shunt) shows the onset of large-amplitude, quasi-periodic fluctuations immediately below 20.6°C . As the temperature decreases further, the system undergoes a second reorganization near 12.0°C , after which the fluctuations collapse into a step-like low-temperature branch. (b) The longitudinal sample voltage $V_{xx}(\text{sample})$ exhibits a parallel restructuring, with oscillatory features developing below 20.6°C and reorganizing again at approximately 12.0°C . The inset shows the zero-lag cross-correlation between I_{xx} and V_{xx} , which displays a strong, narrow peak at lag = 0, indicating coherent coupling between the two longitudinal channels during the temperature-driven dipolar reorganization and serving as an internal measurement-control check. All data were recorded simultaneously at a 1 Hz sampling rate.

two complementary experiments performed on consecutive days using $500 \text{ ng}/\mu\text{L}$ and $100 \text{ ng}/\mu\text{L}$ DNA–water samples, respectively. In Figure 2, the longitudinal channels reveal two clear temperature-driven reorganizations at 20.6°C and 12.0°C , expressed as sharp changes in the fluctuation amplitude and correlation structure of I_{xx} and V_{xx} . In Figure 3, an independent sweep under identical magnetic-field conditions ($B = 500 \text{ mT}$) shows that the transverse channel remains quiet above about 12°C , but below this same temperature, the system reorganizes into a regime of large-amplitude, nearly periodic V_{xy} oscillations exceeding 150 mV . Together, these measurements establish 12°C as a robust temperature boundary where the dipolar ensemble transitions into a strongly coherent, oscillatory state.

Two-stage temperature dependence of coherence

The combined behavior of Figures 2 and 3 reveals a clear, two-stage temperature dependence of coherence in

hydrated DNA. The first restructuring at 20.6 °C, visible only in the longitudinal channels (Fig. 2), marks the onset of enhanced dipolar sensitivity, where thermal agitation becomes sufficiently reduced for correlated hydrogen-bond reorientation to begin. However, the transverse channel remains largely featureless above 12 °C (Fig. 3), indicating that this initial transition does not yet produce a robust, phase-locked polarization mode.

The second transition at 12.0 °C is qualitatively different. Below this temperature, both experiments show a pronounced reorganization: in Figure 2, the longitudinal fluctuations collapse into a low-temperature branch, while in Figure 3 the transverse channel suddenly acquires large-amplitude, nearly periodic oscillations that persist for several degrees of cooling. The simultaneous change in both longitudinal and transverse responses demonstrates that the dipolar network undergoes a collective mode-selection process at 12 °C, entering a regime where cross-channel coherence becomes strong, and the transverse polarization mode dominates the macroscopic response.

Three temperature regimes of dipolar organization

This two-stage progression – initial softening at 20.6 °C followed by full coherence below 12.0 °C – supports the interpretation that temperature tunes the coupling strength and phase ordering of the proton–proton-hole dipolar ensemble. Above 20.6 °C, dipoles fluctuate largely independently; between 20.6 and 12.0 °C, they begin reorganizing but remain only partially correlated; and below 12.0 °C, the system crosses a coherence boundary and forms a stable, collectively oscillating polarization mode. These temperature-dependent reorganizations parallel the field-induced transitions observed elsewhere in the manuscript, reinforcing the view that coherent polarization in hydrated DNA emerges when both magnetic alignment and thermal suppression of decoherence act together to stabilize collective dipolar motion.

Magnetic-field dependence at fixed temperature

Having established the temperature boundaries for coherence (Figs. 2 and 3), we next examine how the transverse polarization responds to magnetic field at fixed, near-room temperature. At a DNA concentration of 500 ng μL^{-1} (Fig. 4), V_{xy} exhibits a sharp threshold at B_c , followed by a staircase of quantized polarization plateaus. The regular spacing of the plateau centers (linear fit $R^2 > 0.99$) persists despite thermal noise of approximately ± 0.1 mV, indicating discrete, field-stabilized configurations of the dipolar network. Control measurements performed on pure water remain featureless under otherwise identical conditions, confirming that quantization requires the DNA-templated hydration architecture. The plateau spacing, together with the oscillation

periodicity analyzed below, yields a consistent coherence density of approximately $4.7 \times 10^{14} \text{ m}^{-2}$, interpreted as the areal density of coherently active dipolar domains. This value reappears independently in the Fourier analysis of the oscillatory regime and in the convergence analysis, supporting a single underlying coherence ensemble. A notable feature of the transverse voltage staircase is the presence of pronounced fluctuations localized at the boundaries between neighboring plateaus. These fluctuations are not uniformly distributed across the signal but appear predominantly in narrow intervals preceding each step. Despite their strength, the system reproducibly settles into a subsequent plateau, indicating that the staircase structure is robust against these fluctuations. Such behavior is characteristic of driven systems undergoing transitions between metastable collective states. Near a stability boundary, competing polarization configurations may become nearly degenerate, leading to enhanced fluctuations as the system explores multiple configurations. Once a new configuration becomes energetically favorable, the system rapidly relaxes into a stable state, giving rise to the next plateau. If the observed steps were dominated by stochastic noise or instrumental artefacts, one would expect the fluctuations to smear out the plateau structure or lead to irregular step spacing. Instead, the fluctuations are confined to the transition regions, while the plateaus themselves remain well defined. This behavior suggests that the fluctuations play an active role in mediating transitions between discrete states rather than obscuring an underlying continuous response. Similar fluctuation-assisted switching phenomena are widely observed in nonlinear and self-organized systems, where noise or thermal agitation enables transitions between neighboring attractors in a multistable landscape.

Oscillatory regime and Landau-like polarization quantization

Lowering the temperature strengthens phase locking among dipoles and reveals SdH-like, $1/B$ -periodic signatures preceding plateau formation. For a DNA concentration of 100 ng μL^{-1} at 5 °C (Fig. 5), both V_{xy} and V_{xx} exhibit robust oscillations periodic in $1/B$ over the field range 0.13–0.30 T. Identical oscillation frequencies in the two channels ($F_{V_{xy}} \approx 6.31$ T and $F_{V_{xx}} \approx 6.27$ T; $\Delta(1/B) = 0.159 \pm 0.002 \text{ T}^{-1}$) indicate a common quantization origin, here attributed to discrete reorganizations of the coherent polarization state rather than charge orbits. FFT-inferred parameters (A_F and k_F , as reported in Fig. 5) quantify the characteristic scale of coherence patterning within the hydration sheet. All 5 °C data were acquired in the same measurement geometry; for reference, the plateaued trace shown in Fig. 4 was recorded at 22.3 °C.

At 6 °C and 500 ng μL^{-1} (Fig. 6), the background-subtracted transverse signal ΔV_{xy} exhibits dense, nearly periodic modulation with a mean spacing of approxi-

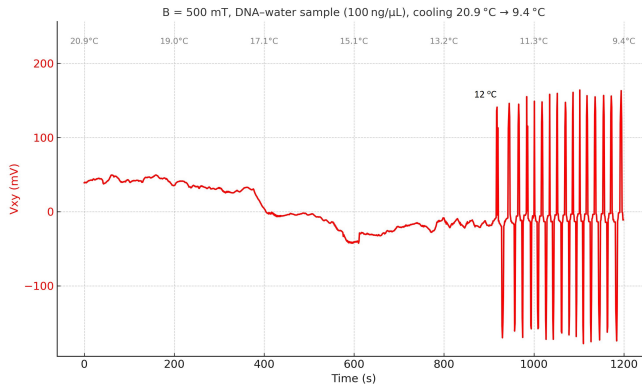


FIG. 3. Temperature-driven onset of large-amplitude transverse polarization oscillations. A cooling sweep from 20.9 °C to 9.4 °C at fixed magnetic field ($B = 500$ mT) shows the evolution of the transverse polarization voltage V_{xy} in a 100 ng/μL DNA–water sample. Above ~ 12 °C, V_{xy} exhibits only small fluctuations and slow drift. Below ~ 12 °C, the response reorganizes abruptly into a regime of large-amplitude, nearly periodic oscillations with peak-to-peak excursions exceeding 150 mV. The oscillations persist over the 12 °C to 9.4 °C interval, consistent with the emergence of a coherent transverse dipolar mode. Temperature stamps above the trace indicate the progression of the cooling sweep. Data were recorded at a sampling rate of 1 Hz.

mately 0.83 T $^{-1}$ and a dominant FFT peak at $F \approx 1.2$ T. Interpreted within the polarization-quantization formalism using an Onsager-type geometric estimator, this yields an effective coherence density of $n_{\text{eff}} \approx 5.8 \times 10^{14}$ m $^{-2}$, consistent with the plateau-derived value obtained near room temperature. The transverse oscillations exceed the longitudinal response by roughly four orders of magnitude and are approximately π out of phase with ΔV_{xx} , as expected for an intrinsically transverse polarization mode with weak dissipation. For $B \gtrsim 0.4$ T, the oscillatory pattern simplifies into broader lobes, indicating a field-driven reorganization into a more globally coherent state.

Polarization-response tensor and crossover to a coherent phase

Converting V_{xx} and V_{xy} to $R_{xx}(B)$ and $R_{xy}(B)$, followed by tensor inversion, yields the polarization-response tensor describing how the longitudinal and transverse channels co-vary under an applied magnetic field (Fig. 7). Both components trace smooth, continuous trajectories rather than exhibiting random scatter, indicating organized dynamics rather than noise-dominated behavior. Above the threshold field, the transverse component becomes dominant and the response evolves into broader, slowly varying lobes, signaling a crossover into a more globally phase-locked dipolar state. This crossover is observed reproducibly under both isothermal conditions and continuous magnetic-field sweeps, supporting

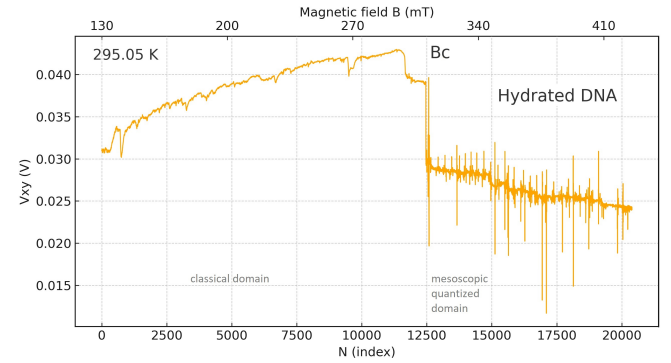


FIG. 4. Threshold behavior and field-induced polarization transition in hydrated DNA. Transverse polarization voltage V_{xy} measured for a 500 ng/μL hydrated genomic DNA sample (pH ≈ 8 , $T = 295.05$ K (21.9 °C)) during a magnetic-field sweep. The lower horizontal axis shows the sweep index N , while the upper axis provides the corresponding magnetic field, which increases approximately linearly from 130 mT at $N = 0$ to 420 mT at $N \approx 20\,000$. At the critical field B_c , the signal exhibits a sharp discontinuity, dropping from about 0.039 V to 0.029 V. This threshold marks the onset of a high-field branch associated with field-induced polarization dynamics in the DNA–water matrix. Beyond this point, the trace displays a slowly descending sequence of discrete, step-like features. Horizontal lines, spaced by approximately 0.8 mV, illustrate the near-regular spacing between effective plateau centers. Two distinct sources of fluctuations are present: (i) broadband noise of roughly ± 0.1 mV distributed along the trace, (ii) localized step-synchronous transients that occur only when the magnet position was manually updated during acquisition, and (iii) importantly, the *enhanced* fluctuations observed at each step do not interrupt the progression of the staircase but instead precede the formation of the next plateau. These transients do not affect the plateau spacing, which remains unchanged across independent sweeps. — full raw data at Zenodo.

its interpretation as an intrinsic feature of the DNA hydration architecture rather than a protocol-dependent effect.

Controls, preparation conditions, and intrinsic origin

Control measurements performed on distilled water (Fig. 8a) show no oscillations, thresholds, or plateau structure, whereas DNA solutions at 1000 and 500 ng μL $^{-1}$ (Figs. 8b and 8c) exhibit the characteristic double-peak motif followed by discrete polarization plateaus. These features are reproducible in both magnetic-field sweep directions (arrows), indicating sweep-direction independence and the absence of hysteresis. Together, these comparisons establish that structured DNA hydration layers are required for the emergence of coherent polarization dynamics.

To assess the role of ionic contributions, we examined unbuffered DNA dissolved directly in distilled water

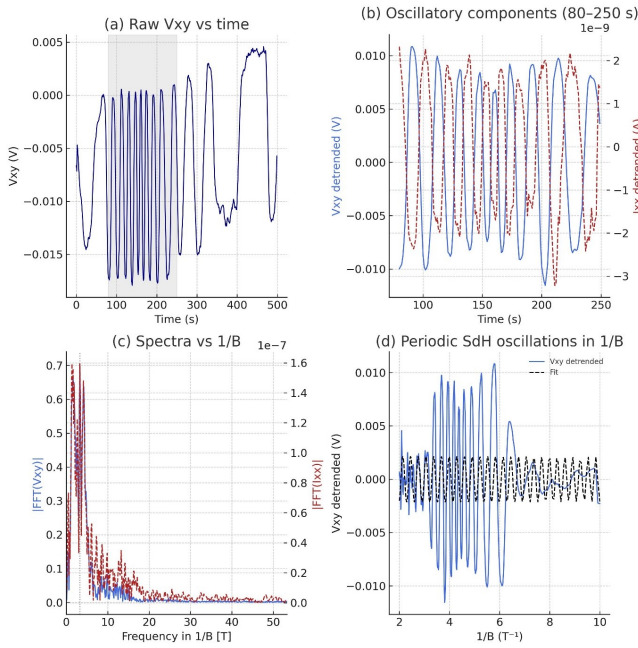


FIG. 5. SdH-like polarization oscillations preceding the threshold (100 ng/ μ L, 5 °C). (a) Transverse polarization voltage V_{xy} recorded in a Greek-cross geometry during a continuous magnetic-field sweep from 0.10 to 0.50 T (0–500 s). (b) Simultaneous longitudinal voltage V_{xx} across a 1 k Ω shunt (with $I_{xx} = V_{xx}/1$ k Ω). Regular oscillations appear between approximately 0.13 and 0.30 T. (c) FFT versus $1/B$ shows a common oscillation frequency in both channels ($F_{V_{xy}} \approx 6.31$ T and $F_{I_{xx}} \approx 6.27$ T; $\Delta(1/B) = 0.159 \pm 0.002$ T $^{-1}$). (d) Oscillatory V_{xx} (proportional to I_{xx}) plotted versus $1/B$ with a sinusoidal fit gives $A_F = (6.0 \pm 0.1) \times 10^{16}$ m $^{-2}$ and $k_F = (1.38 \pm 0.01) \times 10^8$ m $^{-1}$. Identical $1/B$ periodicities in V_{xy} and V_{xx} (FFT) confirm a common polarization-coherence origin. (All data recorded at 5 °C; by contrast, Fig. 4 was acquired at 22.3 °C.)

(Fig. 9). Both the 100 and 480 ng μ L $^{-1}$ samples display a pronounced threshold near $B \approx 0.6$ T (voltage drop > 25 mV), followed by stabilization into Landau-like polarization levels with a spacing of approximately 1 meV, close to the ≈ 0.8 meV value reported previously. This agreement indicates that the observed quantization is intrinsic to the hydrated DNA matrix and does not depend on buffer ions. A Cu-coated control sample exhibits a transverse response of opposite sign, consistent with electronic conduction, further distinguishing the polarization-driven response observed in DNA solutions.

An interference pattern

Beyond the quantized steps and $1/B$ -periodic oscillations, coherent coupling between the longitudinal and transverse polarization channels is directly revealed by the interference reconstruction shown in Fig. 10. By

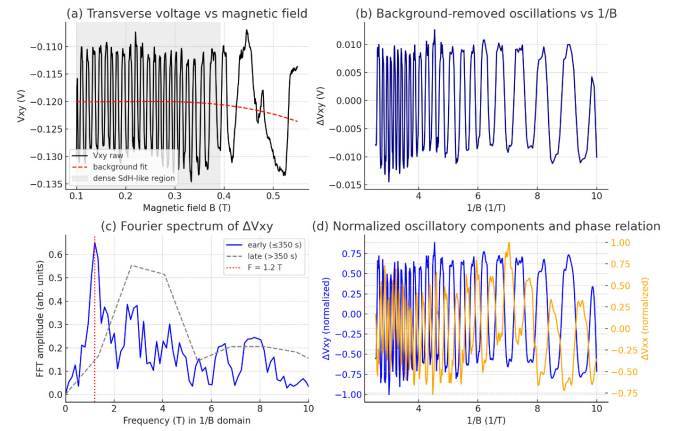


FIG. 6. Low-temperature SdH-like polarization oscillations (6 °C, 500 ng/ μ L). (a) V_{xy} during a 540 s magnetic-field sweep from 0.10 to 0.50 T (RH 29%). Raw data (black) and polynomial background (red dashed) are shown. Dense oscillations dominate for $B \leq 0.40$ T. (b) Background-removed ΔV_{xy} plotted versus $1/B$ shows near-periodic modulation with a mean spacing of approximately 0.83 T $^{-1}$. (c) FFT of ΔV_{xy} in early ($t \leq 350$ s, blue) and late ($t > 350$ s, grey) intervals yields a dominant frequency $F \approx 1.2$ T, corresponding to an effective coherence density $n_{\text{eff}} \approx 5.8 \times 10^{14}$ m $^{-2}$ (Onsager estimator). (d) Normalized ΔV_{xy} (blue) and ΔV_{xx} (orange) plotted on dual axes. ΔV_{xy} exceeds ΔV_{xx} by roughly four orders of magnitude and is approximately π out of phase with ΔV_{xx} , consistent with an intrinsically transverse polarization mode. Above about 0.40 T, the response reorganizes into broader, more coherent lobes.

combining the simultaneously acquired signals $V_{xx}(t)$ and $V_{xy}(t + \tau)$ during a linear magnetic-field ramp, the interference map $S(t, \Delta\phi)$ exhibits alternating constructive and destructive bands whose spacing and contrast remain stable across the entire 100–200 mT interval at 10 °C for 100 ng μ L $^{-1}$ DNA. The region of maximal fringe intensity occurs near $\Delta\phi \approx 200^\circ$, consistent with the independently measured V_{xx} – V_{xy} phase lag and with Lissajous traces obtained under identical conditions (not shown). The persistence and sharpness of these interference fringes indicate that the two channels share a common, phase-coherent polarization mode. In this regime, the system behaves as a coupled dipolar oscillator with a well-defined phase relationship between its longitudinal and transverse components, reinforcing the interpretation that the transverse response originates from coherent polarization dynamics within the DNA–water hydrogen-bond network.

In conventional transport measurements, the longitudinal (V_{xx}) and transverse (V_{xy}) voltages correspond to independent components of the resistivity tensor and do not exhibit phase-coherent coupling. In contrast, the hydrated DNA–water matrix examined here displays a markedly different behavior: V_{xx} and V_{xy} evolve as two quadratures of a single, field-driven collective polarization mode. This coupling reflects the quasi-two-dimensional organization of the hydration environment

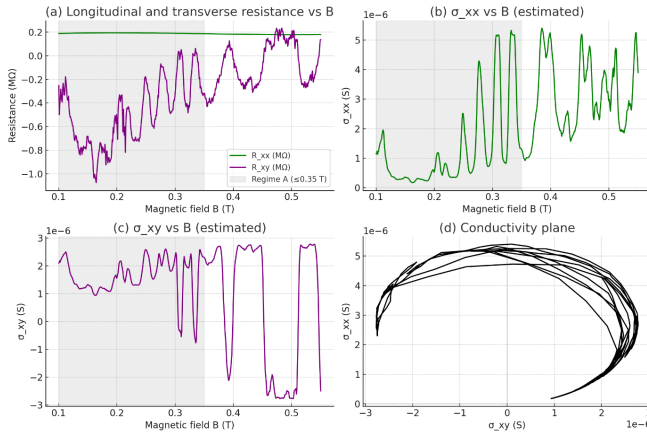


FIG. 7. Field-dependent resistances and polarization-response tensor. (a) R_{xx} and R_{xy} obtained from V_{xx} and V_{xy} using the calibrated current profile. For $B \leq 0.35$ T the traces show dense SdH-like modulation. (b,c) $\sigma_{xx}(B)$ and $\sigma_{xy}(B)$ derived by tensor inversion. Low-field structure collapses above $B_c \approx 0.35$ T into a simplified envelope consistent with a Fröhlich-like coherent polarization mode. (d) Parametric σ_{xx} – σ_{xy} trajectory showing a smooth, reproducible curve, demonstrating an organized and field-driven transformation of the polarization state.

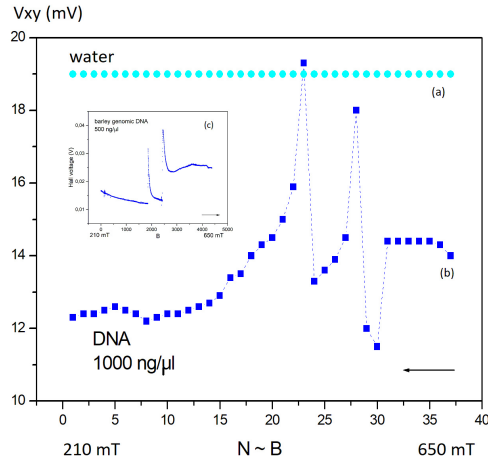


FIG. 8. Controls vs DNA: coherent polarization requires the DNA–water architecture. (a) Transverse polarization voltage V_{xy} : Distilled water shows no oscillatory or quantized features. (b,c) DNA–water at 1000 ng/μL and 500 ng/μL exhibits a reproducible double-peak motif followed by discrete plateaus. Peak positions remain the same in both sweep directions, excluding hysteresis. Coherent polarization is therefore intrinsic to the hydrated DNA matrix. (Full datasets available on Zenodo.)

around DNA, which enables long-range dipolar alignment and supports a coherent oscillatory response under magnetic excitation. The emergence of a stable and reproducible phase relationship between V_{xx} and V_{xy} , persisting across multiple oscillatory cycles and ex-

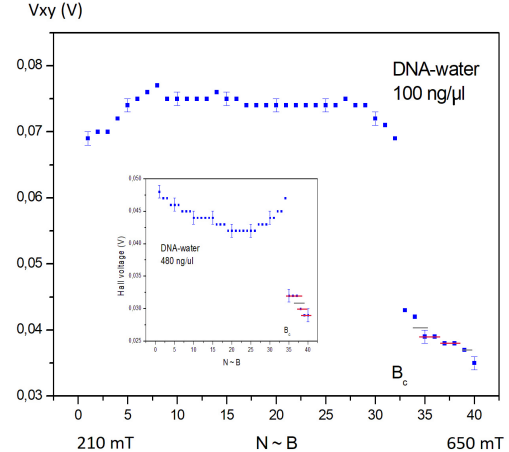


FIG. 9. Quantized polarization in DNA–water without buffer. Main: Transverse polarization voltage V_{xy} for 100 ng/μL DNA dissolved directly in distilled water. Inset: 480 ng/μL sample under identical buffer-free conditions. Both concentrations show a collective threshold near ≈ 0.6 T with a >25 mV drop, followed by stabilization into Landau-like polarization levels (spacing ≈ 1 mV; earlier estimate ≈ 0.8 mV). Red lines mark observed levels; grey indicates partially resolved levels. Quantization is intrinsic to the hydrated DNA matrix and does not require buffer ions.

perimental conditions, indicates that both channels derive from a unified chiral polarization dynamics rather than from independent conductive pathways. Such interference between longitudinal and transverse polarization components is not observed in bulk aqueous systems and appears to arise from the combination of reduced dimensionality, DNA-templated molecular ordering, and magnetic-field-induced symmetry breaking. Together, these results show that the hydrated DNA matrix can sustain a coherent collective vibrational mode whose longitudinal and transverse projections manifest as an interference-like pattern in the measured voltages, revealing an unexpectedly organized polarization response under ambient conditions.

Phase synchronization between transverse voltage and photovoltage

To further assess whether the transverse voltage oscillations reflect a collective dynamical process, we simultaneously recorded an independent photovoltage signal (CH4) under the same magnetic-field and temperature protocols. Figure 11 presents a phase-space representation of the transverse voltage V_{xy} and the photovoltage, revealing strong phase locking between the two signals. The phase agreement exceeds 0.8 over extended intervals, indicating a high degree of synchronization between electrical and photonic observables. This correlation supports the interpretation that the transverse response re-

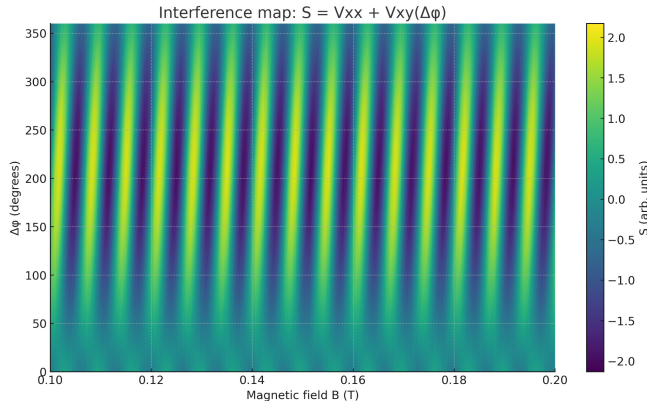


FIG. 10. Interference map constructed from simultaneous V_{xx} and V_{xy} signals. $S(t, \Delta\phi) = V_{xx}(t) + V_{xy}(t + \tau)$ computed during a linear magnetic-field ramp at 10 °C for 100 ng/μL DNA. Alternating constructive and destructive regions form stable interference fringes, with maximal contrast at a well-defined phase offset $\Delta\phi$ visible in the map. The persistence and sharpness of the fringes indicate coherent coupling between the longitudinal and transverse polarization components. The deviation from a perfect 180° anticorrelation is partly attributable to the ~0.25 s sequential sampling delay between V_{xx} and V_{xy} . Although the fringes are not spatial (as in a Young double-slit experiment), they arise from the same principle: coherent superposition of two oscillatory signals. The alternating constructive and destructive regions therefore reflect a stable phase relationship between V_{xx} and V_{xy} , analogous to phase-dependent interference in optical or atomic interferometry.

fects collective polarization dynamics of the DNA–water system.

Consistent behavior is observed during magnetic-field sweeps. Figure 12 shows the transverse photovoltaic response (CH4) recorded concurrently with the electrical measurements during a linear magnetic-field ramp. The photovoltage exhibits a clear transition near the same critical field identified in the electrical channels, marked by a qualitative change from dense, high-amplitude oscillations to a lower-amplitude regime. The appearance of this transition in a physically independent detection channel, spatially separated from the transport contacts, indicates that the magnetic-field-induced reorganization involves the coupled DNA–water system as a whole. Together, these observations reinforce the interpretation that the field-driven transition reflects a system-level collective polarization dynamics.

Convergence of coherence density and unified picture

Independent estimates of the effective coherence density (n_{eff}) obtained from both the oscillatory regime and plateau counting converge. A Shubnikov–de Haas–like analysis gives $n_{\text{eff}} \approx (4.8 \pm 0.5) \times 10^{14} \text{ m}^{-2}$, while the plateau spacing yields $n_{\text{eff}} \approx (4.69 \pm 0.5) \times$

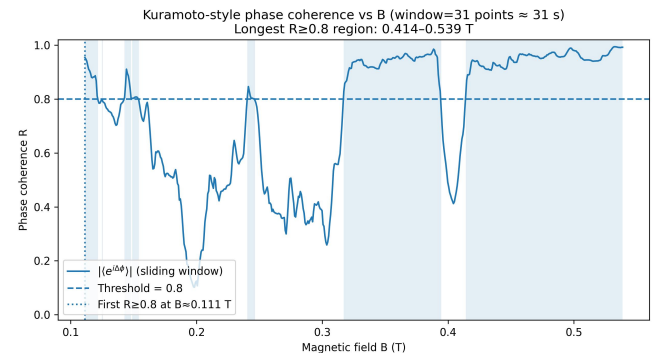


FIG. 11. Phase synchronization between transverse voltage and photovoltage. Phase-space representation of the transverse voltage V_{xy} and a simultaneously measured photovoltage signal (CH4) recorded under the same magnetic-field and temperature protocol. The loop structure and stable trajectory indicate strong phase locking between electrical and photonic observables, with phase agreement exceeding 0.8 over extended intervals. This synchronization supports a collective polarization-dynamics origin of the oscillatory transverse signal rather than an instrumental artifact.

10^{14} m^{-2} . Agreement at the ~2% level indicates that the $1/B$ -periodic oscillations and the quantized polarization plateaus originate from the same field-organized dipolar coherence ensemble. The transition near the critical field marks a crossover from repeated, domain-selective quantization to a more globally phase-locked, Fröhlich-like mode. Control experiments and buffer-free samples confirm that the effect is intrinsic to the DNA hydration architecture.

A phase diagram

The approximate magnetic-field–temperature (B – T) phase diagram shown in Fig. 13 summarizes the regimes of coherent polarization identified across all measurements performed to date. The diagram incorporates magnetic-field thresholds (0.25–0.35 T), two reproducible temperature transitions at 20.6 °C and 12.0 °C, polarization staircases, bands of SdH-like oscillations, and the emergence of low-temperature Fröhlich-type oscillations. Together, these observations delineate three principal domains: (i) a high-temperature incoherent regime without quantization; (ii) an intermediate regime in which discrete polarization plateaus coexist with $1/B$ -periodic oscillations; and (iii) a low-temperature, high-field regime characterized by a globally phase-locked polarization mode. Gaussian blurring was applied during construction to avoid artificially sharp boundaries, reflecting the intrinsic softness and heterogeneity of the hydrogen-bond network. The resulting diagram illustrates how magnetic alignment and thermal suppression of decoherence jointly organize the DNA–water matrix into quantized, and ultimately coherent, polarization states.

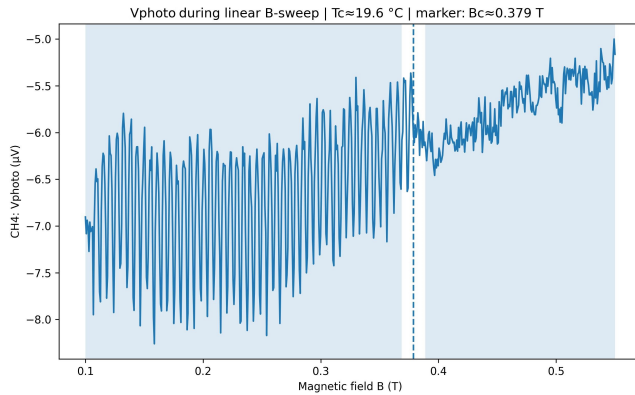


FIG. 12. Photovoltaic response during magnetic-field sweep in hydrated DNA. Transverse photovoltaic signal (CH_4 , V_{photo}) recorded from a photovoltaic plate positioned above a hydrated DNA sample ($5 \mu\text{L}$, $500 \text{ ng } \mu\text{L}^{-1}$) during a linear magnetic-field sweep ($B \approx 0.10\text{--}0.55 \text{ T}$ over 600 s ; sampling interval 1 s). The experiment was performed under ambient laboratory conditions ($T \approx 19.6 \text{ }^{\circ}\text{C}$, relative humidity $\approx 23\%$), with a 0.1 V bias applied to the transport contacts ($CH_1\text{--}CH_3$ recorded simultaneously). A distinct transition occurs near $t \approx 371 \text{ s}$, corresponding to $B_c \approx 0.38 \text{ T}$ under the linear sweep assumption, where the CH_4 signal changes from dense, high-amplitude oscillations to a lower-amplitude regime. This behavior indicates that the field-driven transition observed electrically is mirrored in an independent photovoltaic proxy channel, consistent with a system-level reorganization rather than a single-channel artifact.

III. DISCUSSION

The data presented here show that hydrated DNA, when subjected to moderate magnetic fields under ambient conditions, exhibits a quantized and oscillatory response that is not accounted for by conventional electrical transport. The transverse voltage V_{xy} , previously interpreted as a Hall-like signal, instead reflects a polarization current generated by coherent oscillations of locally neutral proton–proton-hole dipoles within the hydration layer. These findings demonstrate that the DNA–water interface can sustain field-induced coherent polarization dynamics, in which magnetic fields discretize and stabilize collective dipolar modes, producing features analogous to Landau-level quantization.

Earlier reports of staircase-like structures and oscillations [11, 12] remain quantitatively valid; the present work reframes their interpretation while preserving the underlying observations. This perspective is consistent with broader suggestions that biological systems may operate in regimes where coherence or quantum-like vibrational organization plays a functional role [8]. Within this framework, the emergence of quantized plateaus and SdH-like oscillations follows naturally from the quasi-two-dimensional confinement of polarization modes within the hydrated DNA layer.

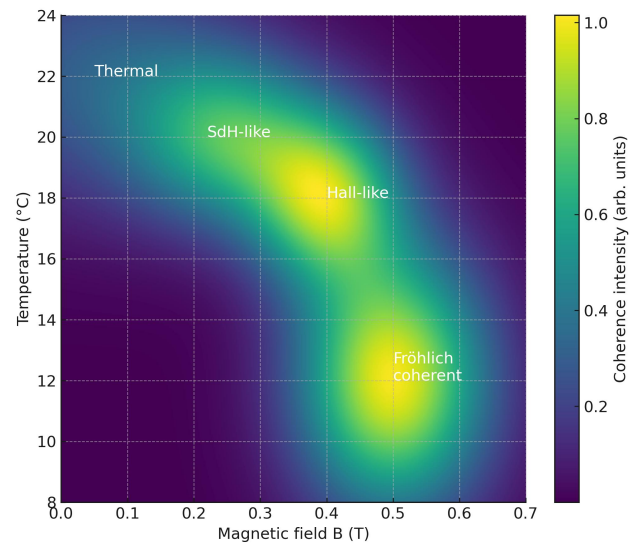


FIG. 13. Field–temperature phase diagram of coherence in hydrated DNA. The diagram summarizes coherent regimes extracted from magnetic-field thresholds ($0.25\text{--}0.35 \text{ T}$), temperature transitions at $20.6 \text{ }^{\circ}\text{C}$ and $12.0 \text{ }^{\circ}\text{C}$, plateau formation, SdH-like oscillation bands, and the emergence of a low-temperature Fröhlich-like mode. Colors represent a qualitative coherence-intensity scale. Boundaries are intentionally smooth to reflect the continuous evolution of the hydrogen-bond network under combined magnetic-field and temperature control.

From transport to polarization coherence

Recasting the observed response in terms of polarization currents resolves conceptual difficulties inherent to charge-transport models. No measurable steady current flows through the sample, yet V_{xy} exhibits a robust structure that scales reproducibly with the magnetic field. This behavior is consistent with a macroscopic polarization mechanism, in which oscillating dipoles embedded in a constrained hydrogen-bond network generate time-dependent electric fields detected as V_{xy} . Within this framework, the observed plateaus correspond to stable configurations of coherent dipolar order, and their spacing reflects the quantization of dipolar orientation states under magnetic torque.

This interpretation is consistent with the microscopic mechanism illustrated in Fig. 1. When a proton transiently hops along a hydrogen bond, it leaves behind a correlated vacancy, forming a locally neutral proton–proton-hole pair. Although electrically neutral, such dipoles are strongly polarizable and can acquire an effective magnetic torque arising from the combination of orbital motion and hydrogen-bond geometry. When many dipoles synchronize through the hydration network, the resulting collective dynamics produce a macroscopic, time-dependent polarization $P(t)$, whose time derivative $J = dP/dt$ gives rise to the observed transverse voltage V_{xy} . This collective polarization mode fits nat-

urally within the framework of Fröhlich-like coherence, corresponding to long-range phase ordering in a driven, dissipative system [1–3].

In this picture, the magnetic field couples to the dipolar ensemble through an effective magnetoelectric interaction. Field-induced torques bias the orientation and phase of proton-proton-hole dipoles, while their collective reorientation feeds back into the macroscopic polarization response. A detailed microscopic magnetoelectric tensor is not required at this stage; it is sufficient that the chiral hydrogen-bond geometry and finite loop areas allow magnetic flux to modulate the phase of the coherent dipolar mode. This mechanism provides a natural route by which moderate magnetic fields can reshape the polarization landscape and enable discrete, quantized reconfigurations of the dipolar ensemble.

Quantization of dipolar modes

The staircase structures observed in V_{xy} and the periodic oscillations in $1/B$ represent two complementary manifestations of the same underlying quantization process. At lower magnetic fields, the dipolar ensemble subdivides into domains that realign sequentially as the field increases, producing SdH-like oscillations in both V_{xy} and V_{xx} . The associated frequencies reflect characteristic coherence areas defined by the structured hydration layer. As the field approaches the critical value near 0.35 T, these domains merge and the system undergoes a sharp transition into a Landau-like regime characterized by quantized polarization plateaus, which constitute the macroscopic signature of field-locked dipolar coherence.

In this regime, the polarization modes can be viewed as quantized angular-momentum states of a collective dipolar field. The quantization arises from coupling between magnetic flux and the effective areas of coherently oscillating dipolar loops, analogous to Onsager-type relations in electronic systems. The extracted coherence densities, consistently in the range $(4.7\text{--}5.8)\times 10^{14} \text{ m}^{-2}$ across SdH-like oscillations, plateau spacing, and tensor inversion, support the presence of a single underlying coherence ensemble. These values correspond to plausible surface coverages of hydrogen-bonded interfacial water, implying coherence domains on the order of several hundred nanometers, in agreement with recent structural studies of confined hydration layers [5].

Transition to a Fröhlich-like coherent phase

Above the threshold magnetic field, the oscillatory structure collapses into broad, slowly varying lobes, indicating a qualitative reorganization of the dipolar ensemble. The discrete domain architecture gives way to a globally phase-locked state in which a large fraction of dipoles oscillate coherently. This Fröhlich-like phase is consistent with a regime in which magnetic alignment

suppresses dominant decoherence pathways, allowing energy injected into local modes to accumulate into a single, collective oscillation [12]. The concomitant flattening of the transverse response (V_{xy}) and the smooth saturation of the longitudinal component (V_{xx}) above the threshold are consistent with a crossover from a domain-based regime to a globally coherent polarization mode.

Such behavior mirrors transitions discussed in classical Fröhlich systems and bears qualitative resemblance to aspects of Bose–Einstein condensation [24, 25], although realized here in a driven, dissipative biological matrix at ambient conditions. The persistence of coherence even when $k_B T$ substantially exceeds the estimated dipolar coupling energies suggests a nontrivial, self-organized mechanism facilitated by nonlinear protonic interactions within the hydrogen-bond network.

Temperature dependence and the coherence boundary

The temperature dependence of the polarization oscillations reveals a coherence boundary near 295 ± 5 K, close to biologically relevant temperatures [10]. With increasing temperature, thermal motion progressively disrupts dipolar phase locking, leading to a suppression of quantized features. Cooling reverses this trend, first restoring discrete oscillations and ultimately yielding fully quantized polarization states at lower temperatures. The amplitudes of the oscillatory components extracted from FFT analysis decay approximately as $\exp(-1/T)$, with activation energies comparable to hydrogen-bond strengths, directly linking the emergence of coherence to the structured hydration network. The appearance of a coherence maximum near physiological temperature suggests that biological hydration layers may naturally operate in a regime optimized by the balance between thermal agitation and collective ordering.

Polarization tensor and phase structure

Simultaneous measurements of V_{xx} and V_{xy} show that the two components are nearly π out of phase. This phase relationship indicates that the transverse voltage arises from an orthogonal rotation of polarization rather than from inductive coupling. When expressed through a polarization-response tensor, the V_{xx} – V_{xy} trajectories trace smooth, Lissajous-like curves, demonstrating a stable dynamical relationship between the longitudinal and transverse components. Such behavior is characteristic of gyroscopic dynamics in magnetized dielectrics and further supports the polarization-current interpretation.

Additional evidence that the magnetic-field-driven transition reflects a collective reorganization of the hydrated DNA system is provided by the photovoltaic response shown in Fig. 12. A qualitatively similar transition appears in this independent proxy channel, which is spatially separated from the electrical contacts. The cor-

respondence between electrical and photovoltaic signatures indicates that the field-induced transition involves a redistribution of polarization dynamics across the DNA–water interface, capable of coupling to both electrical and electromagnetic observables. Although the microscopic origin of the photovoltaic response remains to be clarified, its synchronization with the electrical transition supports the interpretation of a system-level coherent polarization mode.

Controls and intrinsic origin

Control measurements indicate that coherent polarization requires the intact DNA–water architecture. Pure water and desiccated DNA films show no quantized or oscillatory features, whereas both buffered and unbuffered DNA solutions exhibit identical plateau spacings and oscillation frequencies, indicating that the observed response does not depend on ionic transport. Metallic control samples produce transverse signals of opposite sign, consistent with conventional charge conduction rather than polarization rotation. Together, these comparisons support the conclusion that the observed transverse responses arise from coherent dipolar dynamics intrinsic to hydrated DNA.

Unified interpretation and connection to prior work

The findings reported here provide a unified interpretation of several years of experimental observations on hydrated DNA under magnetic fields [11, 12]. Although earlier analyses framed the transverse response in terms of protonic conduction, all quantitative features—critical fields, SdH-like periodicities, plateau spacings, threshold voltages, and inferred coherence densities—remain internally consistent across studies. The present work reinterprets these features as signatures of field-organized dipolar polarization rather than transport by mobile charge carriers. The recurrence of the effective coherence density n_{eff} across independent datasets, including those reported in *Physica B* and *BioSystems*, underscores the robustness of the underlying physical phenomenon.

Interference mapping as a probe of coherence

The interference pattern shown in Fig. 10 provides direct evidence of coherent coupling between the longitudinal and transverse polarization channels. By combining the simultaneously acquired signals V_{xx} and time-shifted V_{xy} into the interference map $S(t, \Delta\phi)$, we observe alternating regions of enhanced and suppressed amplitude that depend sensitively on their relative phase. These structured bands arise from the superposition of two phase-locked oscillatory components and reflect the in-

stantaneous phase relationship between the longitudinal and transverse polarization dynamics.

The region of maximal fringe contrast near $\Delta\phi \approx 200^\circ$ corresponds closely to the independently measured phase lag between V_{xx} and V_{xy} . The stability, sharpness, and persistence of the interference fringes across the full magnetic-field interval indicate that the two channels do not fluctuate independently, but instead remain locked to a common dynamical mode. In this regime, the hydrated DNA system behaves as a coupled dipolar oscillator with a well-defined phase structure linking its longitudinal and transverse polarization components. The interference reconstruction therefore serves as a sensitive probe of macroscopic phase coherence in the polarization response, reinforcing the interpretation that the transverse voltage originates from a collective, coherently organized polarization mode rather than from uncorrelated fluctuations.

The polarization Hall effect in hydrated DNA

Transverse responses carried by neutral excitations have become a central theme in modern condensed-matter physics. Recent demonstrations of the phonon Hall effect, including a recent *Phys. Rev. Lett.* report [22], show that neutral vibrational excitations can generate measurable transverse voltages in insulating crystals. This growing body of work, encompassing phonon thermal Hall effects [16, 26–28], magnon Hall currents [17], and exciton Hall responses [18], establishes that Berry curvature, chiral geometry, and broken inversion symmetry can produce Hall-like phenomena in the absence of charge transport.

The observations reported here naturally align with this emerging paradigm of transverse responses mediated by neutral excitations. Earlier interpretations framed the measured transverse voltage V_{xy} as evidence for a protonic Hall effect, implicitly invoking long-range proton conduction. Here, we adopt a more conservative and physically grounded interpretation, in which hydrated DNA supports a strongly polarizable network of proton fluctuations and hydrogen-bond vibrations that can, under suitable conditions, organize into coherent polarization modes. Within this framework, the intrinsic chirality of DNA and its structured hydration environment provide a plausible route for magnetic-field-induced transverse polarization responses without invoking itinerant charge transport. The reproducible voltage threshold near 40–50 mV is interpreted as a crossover into a regime of enhanced collective coherence, above which transverse oscillations with stable phase and amplitude become observable.

Chirality, geometry, and collective response

DNA's intrinsic chirality plays a central role in shaping the observed transverse response. The helical geometry imposes well-defined geometric phase relations on protonic and vibrational excitations, analogous to mechanisms proposed for chiral phonon and magnon Hall effects. When coupled to a magnetic field, this chiral organization can generate transverse polarization components even in the absence of charged carriers. This framework reconciles earlier interpretational ambiguities, accommodates the full set of observed features, and situates hydrated DNA within a broader class of soft-matter systems exhibiting Hall-like responses mediated by neutral excitations.

Protonic polarization modes

Viewed through this lens, the polarization Hall effect reflects a broader principle: soft, hydrogen-bonded matter can support magnetically induced transverse responses mediated by coherent polarization waves. This perspective points to an emerging area of study—*protonic polarization physics*—focused on the coherence, geometry, and controllability of proton-mediated polarization modes in aqueous and biological environments. Related concepts may connect the dynamics of hydrated DNA to coherent energy-transfer phenomena observed in photosynthetic complexes [29, 30] and to other forms of water-mediated collective behavior.

The observed phase locking between the transverse voltage and an independently measured photovoltage provides additional support for a collective polarization dynamics underlying the oscillatory response. Together, these findings establish a framework for quantized polarization coherence in soft matter that bridges molecular biology and quantum condensed-matter physics. Future investigations should explore the roles of hydration level, magnetic-field orientation, external bias, and time-resolved spectroscopy. The interplay between molecular geometry, hydrogen-bond topology, and magnetic coupling may reveal new pathways to room-temperature coherence in biological systems. In this context, hydrated DNA emerges as a representative platform in which collective dipolar order can be magnetically stabilized under physiologically relevant conditions.

IV. CONCLUSION

The experiments reported here establish hydrated DNA as a field-stabilized and temperature-gated coherent dipolar system. Moderate magnetic fields and controlled cooling reorganize the hydration layer into discrete, quantized polarization states and, at lower temperatures, into robust oscillatory modes. The observed

staircase-like transitions, well-resolved $1/B$ -periodic oscillations, and large-amplitude transverse responses are not consistent with conventional ionic or electronic transport. Instead, they arise from the collective dynamics of proton–proton-hole dipoles within the hydrogen-bond network, whose synchronized motion generates a measurable polarization current.

Across all magnetic-field and temperature regimes investigated, the effective coherence density (n_{eff}) remains remarkably consistent, converging to approximately $(4.7\text{--}5.8) \times 10^{14} \text{ m}^{-2}$ regardless of DNA concentration, sweep protocol, or sample history. This reproducibility, together with the characteristic π phase relation between longitudinal and transverse channels, indicates that the quantized and oscillatory features originate from a single, architecture-defined dipolar ensemble. The reproducible temperature thresholds at $20.6 \text{ }^{\circ}\text{C}$ and $12.0 \text{ }^{\circ}\text{C}$ further demonstrate that coherence can be tuned along two independent control axes, with magnetic alignment and thermal suppression of decoherence acting cooperatively to stabilize macroscopic polarization order.

These findings identify the DNA–water interface as a biologically relevant soft-matter system capable of sustaining coherent dipolar dynamics near ambient conditions. They connect the present observations to broader themes in biophysics, including cooperative proton transfer, hydration-layer structuring, and long-range polarization behavior in proteins, membranes, and photosynthetic complexes. The emergence of quantized and coherent polarization in hydrated DNA opens pathways for systematic exploration of dipolar modes in biological matter, including frequency-resolved spectroscopy, spatial mapping of coherent domains, and controlled perturbations using temperature, magnetic field, and hydration geometry.

Overall, hydrated DNA emerges as a natural platform in which magnetic field and temperature jointly organize a hydrogen-bond network into a coherent, quantized polarization state. This work provides a conceptual framework for understanding polarization dynamics in living matter and establishes a foundation for future investigations of coherence in soft and biological quantum materials. By demonstrating that hydrated DNA can support field-stabilized and temperature-dependent collective polarization dynamics under physiologically relevant conditions, these results highlight a potential connection between concepts developed in condensed-matter physics and emerging questions in biophysics and quantum biology, and suggest that coherent polarization may play a broader organizational role in structured soft matter.

METHODS

Sample preparation

Barley genomic DNA (double-stranded, isolated using the CTAB method, modified after Doyle and Doyle [31])

was dissolved in TE buffer (pH 8, containing Tris–HCl and EDTA). Working concentrations were 100, 500, and 1000 ng μL^{-1} . Prepared DNA solutions were stored at -20°C between experiments to minimize degradation.

For all measurements, a 5 μL droplet was placed onto a planar four-contact Cu-coated substrate defining an active area of approximately $0.7 \times 0.7 \text{ cm}^2$. Surface tension, together with a microscope glass coverslip, confined the hydration volume to a quasi-two-dimensional layer. The resulting hydrated film thickness was approximately $10 \pm 2 \mu\text{m}$. Samples were equilibrated at controlled relative humidity (25–35%) to ensure a reproducible semi-hydrated state. Control measurements were performed on pure water, buffer-free DNA solutions, and metallic Cu-coated substrates.

Magnetic-field generation and calibration

Magnetic fields in the range 0.05–0.65 T were generated using NdFeB permanent magnets mounted on a motor-driven linear translation stage that controlled the magnet–sample separation. The system operated in two modes: a motor-sweep mode ($0.1\text{--}0.5 \text{ mT s}^{-1}$) for high-resolution oscillation and plateau measurements, and a manual mode for threshold measurements to minimize potential electromagnetic interference from the motor. Magnetic-field values were calibrated before each measurement session using a Hall-probe gaussmeter with an accuracy of $\pm 1 \text{ mT}$. All fields were applied perpendicular to the sample plane.

Temperature control

Temperature-dependent experiments were conducted in a refrigerated enclosure equipped with two ice reservoirs to provide passive thermal stabilization. A calibrated Extech thermometer (accuracy $\pm 0.1^\circ\text{C}$) was positioned within 5 mm of the sample. Typical cooling rates were $0.01\text{--}0.03^\circ\text{C s}^{-1}$. Two reproducible temperature-driven reorganizations were consistently detected near 20.6°C and 12.0°C . Ambient relative humidity was maintained within $\pm 3\%$ to ensure stable hydration conditions during temperature sweeps.

Electrical measurement geometry

A 0.1 V DC source was applied through a $1 \text{ k}\Omega$ shunt resistor, defining the longitudinal current channel. Signals were recorded using four synchronized acquisition channels:

- CH1: longitudinal voltage V_{xx} across the $1 \text{ k}\Omega$ shunt (yielding $I_{xx} = V_{xx}/1 \text{ k}\Omega$),
- CH2: longitudinal sample voltage V_{xx} (sample),

- CH3: transverse voltage V_{xy} (sample),
- CH4: photovoltage (when measured).

Magnetic-field sweep experiment shown in Fig. 4 was sampled at 740 Hz, yielding approximately 10^5 data points per trace. The remaining magnetic-field and temperature sweeps were sampled at 1 Hz. All measurement electronics were battery-powered and magnetically shielded to minimize inductive coupling.

Photovoltage measurement

In selected experiments, an independent photovoltage channel (CH4) was recorded simultaneously with the electrical measurements. A photovoltaic plate was positioned horizontally behind the hydrated DNA sample, at a distance of approximately 3 cm from the sample, and outside the region between the magnet and the sample. The plate was not electrically connected to the transport circuitry. Photovoltage was measured directly at the plate terminals using a dedicated acquisition channel. This configuration ensured both physical and electrical separation between the photovoltage detection and the transport contacts, allowing the photovoltage to serve as an independent proxy for field-induced dynamical reorganization of the DNA–water system.

Data acquisition and signal processing

Raw V_{xy} traces were detrended using low-order polynomial subtraction to remove slow background drift associated with hydration dynamics and thermal equilibration. The resulting ΔV_{xy} signal was analyzed in both magnetic-field and time domains.

Fast Fourier transform (FFT) analysis employed a Hann window with amplitude normalization. Forward and reverse magnetic-field sweeps were compared to verify periodicity. Dominant oscillation frequencies were typically observed near $F \approx 1.2 \text{ T}$ at low temperature and $F \approx 6.3 \text{ T}$ near room temperature. Cross-channel correlation between I_{xx} and V_{xx} was used to identify synchronous longitudinal polarization events.

Phase relationships between V_{xx} and V_{xy} were extracted using Hilbert transforms, revealing near- π phase shifts in oscillatory regimes. Because V_{xx} and V_{xy} were acquired sequentially through a multiplexer, a sampling offset of approximately 0.25 s was introduced and taken into account in phase analysis. Hilbert-phase analysis was further used to estimate the phase-coherence length, yielding approximately 55 nm at room temperature and more than 100 nm at temperatures below 15°C . These values are consistent with earlier Gross–Pitaevskii simulations of the dipolar ensemble.

Extraction of effective coherence area and density

The periodicity in $1/B$ was converted into a characteristic dipolar coherence area using an Onsager-type geometric estimator,

$$A_F = \frac{2\pi e}{\hbar} F, \quad n_{\text{eff}} = \frac{A_F}{2\pi}.$$

The appearance of the elementary charge e in this Onsager-type estimator reflects its standard geometric form and does not imply electronic carriers in the present polarization-based interpretation.

This expression was used solely to estimate the characteristic spatial scale of coherent dipolar domains and not to infer electronic carrier density. Independent estimates derived from FFT periodicity, plateau spacing, and comparisons across measurement protocols consistently yielded $n_{\text{eff}} \approx (4.7\text{--}5.8) \times 10^{14} \text{ m}^{-2}$, indicating a single field-organized dipolar coherence ensemble.

Control experiments

Control measurements demonstrated that pure water exhibited no oscillations, thresholds, or plateau structures. Desiccated DNA films and metallic films displayed no coherent features, whereas metallic Cu controls produced opposite-sign transverse signals characteristic of conventional electronic Hall responses. Buffer-free DNA samples yielded the same plateau structure and oscillation periodicity as buffered samples, indicating that ionic conduction does not contribute to the observed signals. Reversing the magnetic-field sweep direction produced identical spacings and frequencies, indicating sweep-direction independence. Together, these controls establish that the observed transverse voltages originate from collective polarization dynamics of the structured DNA hydration layer.

Phase-diagram construction

The magnetic-field-temperature (B - T) phase diagram was constructed using magnetic-field thresholds near 0.25–0.35 T, temperature transitions at 20.6 °C and 12.0 °C, polarization plateau structures, SdH-like oscillation bands, and the onset of low-temperature Fröhlich-type oscillations. Gaussian blurring was applied to avoid artificially sharp boundaries, yielding a continuous representation of coherent dipolar regimes.

DATA AVAILABILITY

All data supporting the findings of this study are openly available. The complete transverse voltage dataset for Fig. 4 (approximately 100,000 data points)

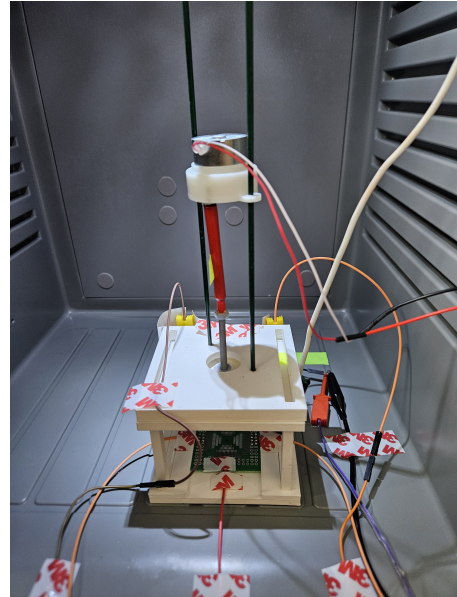


FIG. 14. Supplementary Figure S1: Custom detector for field-induced polarization measurements in hydrated DNA. A $\sim 5 \mu\text{L}$ DNA–water sample was deposited at the center of a single-sided printed-circuit board ($40.5 \times 43 \text{ mm}$) and sealed with a glass cover in a van der Pauw-type configuration. The resulting quasi-two-dimensional hydrated layer (thickness $\approx 10 \mu\text{m}$; see Methods) was contacted via an inner ring of copper-tipped, tin-free ohmic contacts ($\sim 0.1 \mu\text{m}$ thick). Black contacts supplied the bias voltage (V_{bias}), magenta contacts monitored the longitudinal potential (V_{xx}), and yellow contacts recorded the transverse polarization response (V_{xy}) arising from field-induced collective dipolar oscillations. A perpendicular magnetic field (B) was applied using permanent neodymium magnets. The detector assembly was housed inside an adiabatically isolated Faraday cage placed in a refrigerator to minimize thermal drift and electromagnetic interference. The magnetic field was varied either continuously (motor-driven screw with clutch) or stepwise (manual or electronically controlled), with the number of turns (index N) calibrated to the magnetic-field induction.

is deposited on Zenodo and can be accessed via the DOI 10.5281/zenodo/1212_121326_8. Additional raw data, processed data, and plotting scripts are available from the corresponding author upon reasonable request.

ACKNOWLEDGEMENTS

The author acknowledges the use of a Keithley DMM6500 multimeter, originally obtained through a joint study with Marek Marzec, published in Scientific Reports. This work was supported by the National Science Centre, Poland (grant no. 2020/37/B/NZ3/03696). The author also thanks Katarzyna Konopka for providing the DNA–water samples.

SUPPLEMENTARY INFORMATION

Note on interference and instrumental artifacts

A potential concern is whether the interference structure reconstructed from the longitudinal and transverse channels could arise from inductive cross-talk or other electromagnetic pickup within the measurement circuitry. In the analysis used here, the interference map is constructed from simultaneously recorded signals as

$$S(t, \Delta\phi) = V_{xx}(t) + V_{xy}(t + \tau), \quad (1)$$

where τ is an applied time shift and $\Delta\phi$ denotes the corresponding effective phase offset (for a narrowband oscillation at angular frequency ω , one may identify $\Delta\phi \approx \omega\tau$).

In a conventional inductive scenario, a spurious voltage would be expected to scale with the time derivative of the driving current, $V_{\text{ind}} \propto dI/dt$, with its phase and amplitude determined primarily by wiring geometry and circuit impedances. By contrast, the transverse signal observed here is consistent with a polarization current generated by collective dipolar dynamics, $J_{\text{pol}} = dP/dt$, whose associated electric field is detected as the transverse voltage V_{xy} . Several observations distinguish these scenarios. First, the interference fringes persist across a range of magnetic-field sweep rates and temperatures and do not correlate with dI/dt , remaining visible even when the longitudinal current varies only weakly. Second, the reconstructed $S(t, \Delta\phi)$ exhibits a reproducible maximum near $\Delta\phi \approx 200^\circ$, consistent with the indepen-

dently extracted phase lag between V_{xx} and V_{xy} obtained via Hilbert analysis; a fixed inductive pickup would instead impose a wiring-defined phase relation that does not systematically evolve with the sample state. Third, identical wiring and acquisition settings applied to control samples (pure water, desiccated DNA, and metallic films) do not yield comparable fringe structures, indicating that the effect is not a generic property of the measurement chain. Fourth, in the oscillatory regime, the transverse response exceeds the longitudinal modulation by several orders of magnitude and is approximately π out of phase with it, a behavior difficult to reconcile with derivative-like inductive pickup, which is typically weak and tightly constrained by circuit coupling. Finally, a corresponding field-driven transition is observed in an independent photovoltage channel that is spatially separated from the electrical contacts and therefore not susceptible to electrical cross-talk in the transport leads. Taken together, these observations support the conclusion that the interference fringes reflect coherent coupling between longitudinal and transverse components of a collective polarization mode intrinsic to the hydrated DNA–water system, rather than inductive or instrumental artifacts. Moreover, the observation of a concomitant field-driven transition in the independently recorded photovoltage V_{photo} strengthens this interpretation, as it demonstrates that the interference pattern reflects a system-level polarization reorganization rather than an artifact confined to the electrical measurement circuitry.

[1] H. Fröhlich, International Journal of Quantum Chemistry **2**, 641 (1968).

[2] H. Fröhlich, *Biological Coherence and Response to External Stimuli* (Springer-Verlag, Berlin, 1988).

[3] A. S. Davydov, Journal of Theoretical Biology **66**, 379 (1979).

[4] S. Hammes-Schiffer, Chemical Reviews **106**, 962 (2006).

[5] D. Donadio and G. Galli, Nature Chemistry **17** (2025), in press.

[6] J. R. Reimers, Proceedings of the National Academy of Sciences **106**, 4219 (2009).

[7] Á. R. Vasconcellos, G. Krein, and M. P. de A. Mello, Information **3**, 601 (2012).

[8] J. Al-Khalili and J. McFadden, *Life on the Edge: The Coming of Age of Quantum Biology* (Bantam Press, London, 2015).

[9] M. Tegmark, Physical Review E **61**, 4194 (2000).

[10] M. Pietruszka and M. Marzec, Scientific Reports **14**, 18592 (2024).

[11] M. Pietruszka, Physica B: Condensed Matter **716**, 417672 (2025).

[12] M. Pietruszka, BioSystems **256**, 105564 (2025).

[13] D. Shoenberg, *Magnetic Oscillations in Metals* (Cambridge University Press, Cambridge, 1984).

[14] D. C. Tsui, H. L. Stormer, and A. C. Gossard, Physical Review Letters **48**, 1559 (1982).

[15] K. von Klitzing, G. Dorda, and M. Pepper, Physical Review Letters **45**, 494 (1980).

[16] C. Strohm, G. L. J. A. Rikken, and P. Wyder, Physical Review Letters **95**, 155901 (2005).

[17] Y. Onose *et al.*, Science **329**, 297 (2010).

[18] K. F. Mak, D. Xiao, and J. Shan, Nature Photonics **12**, 451 (2018).

[19] T. Saito, H. Ochoa, and M. S. Dresselhaus, Physical Review Letters **123**, 065901 (2019).

[20] X. Li, B. Fauqué, Z. Zhu, and K. Behnia, Nature Communications **14**, 1027 (2023).

[21] X.-T. Zhang, Y. H. Gao, and G. Chen, Physics Reports **1070**, 1 (2024).

[22] X. Jin *et al.*, Physical Review Letters **135**, 196302 (2025).

[23] S. A. Owerre, Journal of Physics: Condensed Matter **28**, 386001 (2016).

[24] M. H. Anderson, J. R. Ensher, M. R. Matthews, C. E. Wieman, and E. A. Cornell, Science **269**, 198 (1995).

[25] W. Ketterle and H.-J. Miesner, Proceedings of the International School of Physics “Enrico Fermi” **140**, 67 (1999).

[26] G. Grissonnanche *et al.*, Nature **571**, 376 (2019).

[27] X. Zhang *et al.*, Nature Physics **19**, 1517 (2023).

[28] Q. Xiang, X. Li, X. Guo, K. Behnia, and Z. Zhu, arXiv (2025), arXiv:2511.08932 [cond-mat.str-el].

- [29] G. S. Engel, T. R. Calhoun, E. L. Read, T.-K. Ahn, T. Mančal, Y.-C. Cheng, R. E. Blankenship, and G. R. Fleming, *Nature* **446**, 782 (2007).
- [30] G. Panitchayangkoon *et al.*, *Proceedings of the National Academy of Sciences* **107**, 12766 (2010).
- [31] J. J. Doyle and J. L. Doyle, *Phytochemical Bulletin* **19**, 11 (1987).